Numerical optimization of gold-dielectric nanoparticle heterostructures for surface plasmon resonance engineering

Kyongsik Choi*, Peter Zijlstra, James W. M. Chon, and Min Gu*

Center for Micro-Photonics, Faculty of Engineering and Industrial Sciences,
Swinburne University of Technology
P.O. Box 218, Hawthorn, Victoria 3122, Australia

ABSTRACT

Metallic nanoparticles are a very attractive and fascinating material due to their multifunctional properties, such as surface plasmon resonance absorption and excitation band tuning. In particular, these properties are proved to be valuable in photothermal therapeutic applications, where the tunable, efficient near-field enhanced ablation or photothermal energy conversions can be used to destroy cancerous cells. A similar mechanism can be applied for three-dimensional multilayer nanopatterning of polymer matrix doped with NPs, where the field enhancement and photothermal energy conversion are utilised to produce micro-explosions and voids. Previously, it was reported that engineering the morphology of nanoparticles (rod and shell shape) can greatly enhance the field enhancement and photothermal conditions. Here, we numerically study the field enhancement efficiencies of nanparticles with heterogeneous morphologies (such as metal - dielectric - metal core-shell structures), and compare their efficiencies to conventional nanosphere and nanoshell structures. Unlike the previous approximate analytical models, the SPR excitation and field enhancement efficiencies are numerically simulated, using the frequency-dependent finite-difference time domain method under tightly focused ultrashort pulse laser irradiation to accurately emulate the experimental conditions.

Keywords: surface plasmon resonance, metal nanoparticles, FDTD, nanofabrication.

1. INTRODUCTION

Surface plasmon resonance (SPR) is an active area of research in near-field nano-photonics and has many potential applications such as sensing, photodynamic therapy, optical circuits, and high resolution microscopy [1-8]. The SPR phenomenon can be observed when a planar or focused light is incident on the surface of metal at a specific boundary condition. In metallic nanoparticles (NPs) the SPR conditions are more size and geometry dependent. Their easy SPR absorption and excitation band tuning covering wavelength ranges from the ultraviolet to optical communication in NIR, provide much more freedom in engineering plasmonic devices [7,8]. In addition, metallic NPs provide highly localized SPR effect, which could be used in enhanced surface ablation or photo-thermal energy conversions as an active or passive heat sensitizer. Until now, the morphological variation resulted rod, cube, core-shell and other structures, and each specific shape has their own merits in certain applications. In this paper, we characterize the highly localized near-field SPR enhancement in metal-dielectric-metal hetero nanoparticle structure and compare it with conventional sphere and shell structures using finite-difference time domain (FDTD) technique.

The SPR excitation in NPs can be rigorously simulated by the well-known Maxwell's electromagnetic (EM) coupling equations with known boundary conditions. There are several numerical methods of solving for EM fields for any arbitrary geometry, such as Green's function method [9], the multiple multipole method [10], and the finite-difference time domain (FDTD) technique [11]. In particular the FDTD method has been attracting interests as a time-domain computational solution of Maxwell equations. The FDTD method has also been widely used for analyzing the EM phenomena in all range of frequencies from microwave to x-ray optics, and in various applications such as near-field

* Correspondence: Email: kchoi@swin.edu.au, mgu@swin.edu.au; Tel: +61-3-9214-4323, Fax: +61-3-92145435

Nanophotonics II, edited by David L. Andrews, Jean-Michel Nunzi, Andreas Ostendorf,
Proc. of SPIE Vol. 6988, 69880R, (2008) · 0277-786X/08/$18 · doi: 10.1117/12.780764

optics [12, 13], photonic crystal [14] and lasing [15], optical tweezer [16], scattering from cells [17], optical storage [18], and diffractive optics [19]. Here, we utilize two dimensional frequency-dependent FDTD method to characterize the absorption and near-field enhancement of hetero-structured gold-dielectric NP structures. This could be useful in photothermal applications or low threshold surface ablations.

2. FREQUENCY-DEPENDENT FDTD

The FDTD method, as one of most powerful computational methods in EMs, has been widely used to model the wave propagation, scattering, and radiation since it was first introduced by Yee [20] in 1966. The EM problems can be solved by integrating the following Maxwell's differential equations for an arbitrary geometry in two-dimensional (2D) space.

$$\nabla \times \vec{E} + \mu_0 \frac{\partial \vec{H}}{\partial t} = 0, \qquad \nabla \times \vec{H} - \frac{\partial \vec{D}}{\partial t} = 0, \qquad \vec{D}(t) = \varepsilon_0 \varepsilon_r \vec{E}(t). \tag{1}$$

The space is divided into small units called Yee cells. Complex dielectric constants are assigned to each cell for given materials. The FDTD method calculates the EM fields in each cell by integrating the Maxwell's equations in a "leap-frog" procedure until the steady state is reached. In the case of a sinusoidal plane wave excitation source, the steady state is reached when all scattered fields vary sinusoidally in time. In order to obtain an accurate field distribution for a 2D object, the cell size must be much less than the size of relevant features because the FDTD algorithm is stable only if $\Delta t \le \Delta u / \left(c\sqrt{2}\right)$, where Δu is the size of a cubic cell and c is the speed of light. In our case we used the cell size of 2 nm and the extremely short time step $\Delta t = 8.3391 \times 10^{-18} s$, which sufficiently satisfies the stability condition.

The analytical solutions require only the material's topology and frequency-dependent index of refraction $\tilde{\varepsilon}(\omega)$ with the real part representing the index of refraction and the imaginary part the extinction coefficient. The optical constants and properties are available in the literature [21,22]. Recent advances have extended the use of FDTD to the treatment of materials with frequency-dependent, complex dielectric constants. Up to now, three major frequency-dependent FDTD methods have been proposed: piecewise-linear recursive convolution (PLRC) [23,24], auxiliary differential equation (ADE) [25], and Z-transform [26]. In this paper we used the PLRC method using Eq. (2). The optical properties of real metals are generally characterized by this frequency-dependent dielectric permittivity and the time-domain electric flux density $\vec{D}(t)$. It is related to the time-domain electric field intensity $\vec{E}(t)$ by the convolution.

$$\vec{D}(t) = \varepsilon_0 \vec{E}(t) + \varepsilon_0 \int_{\tau=0}^{t} \vec{E}(t-\tau)\chi(\tau)\, d\tau, \tag{2}$$

where the susceptibility $\chi(\tau)$ is the inverse Fourier transform of $\tilde{\chi}(\omega) = \varepsilon_0 \left(1 + \tilde{\varepsilon}(\omega)\right)$, and ε_0 and $\tilde{\varepsilon}(\omega)$ are the permittivity of free space and the frequency-dependent complex permittivity function of the metal. The complex dielectric function is critical to the optical properties of metal-dielectric system. For noble metals, it can generally be described by Lorentz-Drude (LD) [27] model with the intra-band (free-electron) effects and inter-band (bound-electron) effects. A complicated function like Eq. (3) for the dielectric dispersion of Au material can be adopted to approximate the measured dielectric function over a wide wavelength range.

$$\tilde{\varepsilon}(\omega) = 1 - \frac{\omega_p^2}{\omega^2 + i\Gamma\omega} - \sum_j^k \frac{f_j \omega_p^2}{\omega_j^2 - \omega^2 + i\omega\Gamma_j}, \tag{3}$$

where ω_p denotes the plasma frequency and Γ_j means the damping coefficients at the resonance frequencies f_j of a metal material. However, in the frequency range of interest (photon energy of 0.82 ~ 4.5 eV), a Drude [28] model is easier to describe and simple to calculate the complex dielectric response of Au. From the experimentally obtained *n-k*

relation we can calculate the following frequency-dependent optical constants $\tilde{\varepsilon} = \varepsilon_{r1} + j\varepsilon_{r2}$ ($\varepsilon_{r1} = n^2 - k^2$, $\varepsilon_{r2} = 2nk$) , $R = \left|\frac{\tilde{n}-1}{\tilde{n}-1}\right|^2 = \frac{(n-1)^2 + k^2}{(n+1)^2 + k^2}$, $\sigma_{AC}(\omega) = \frac{\sigma_0}{1 - i\omega\Gamma}$, and $\omega_p = \omega\sqrt{\frac{(1-\varepsilon_{r1})^2 + \varepsilon_{r2}^2}{1-\varepsilon_{r1}}}$, $\Gamma = \omega\frac{\varepsilon_{r2}}{1-\varepsilon_{r1}}$ using a proper fitting method [29]

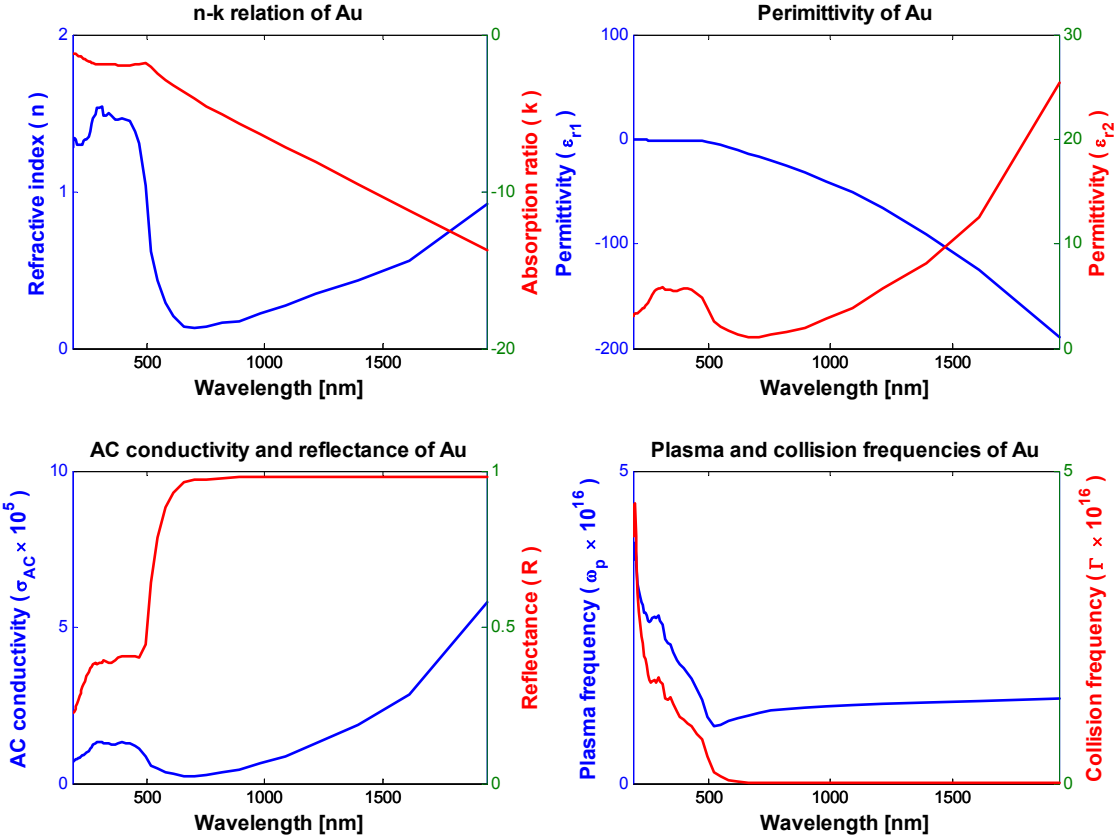

Fig. 1. Frequency-dependent optical constants of Au material: (a) *n-k* relation, (b) complex dielectric function $\tilde{\varepsilon}(\omega) = \varepsilon_{r1} + i\varepsilon_{r2}$, (c) reflection coefficient $R(\omega)$ and AC conductivity $\sigma_{AC}(\omega)$, and (d) plasma frequency $\omega_p(\omega)$ and damping frequency $\Gamma(\omega)$.

Figure 1 shows the calculated frequency-dependent complex dielectric function, AC conductivity $\sigma(\omega)$, reflectance $R(\omega)$, plasma frequency $\omega_p(\omega)$, and damping coefficient $\Gamma(\omega)$ with respect to the wavelength variation from the experimentally obtained *n-k* values of Au material [29].

The 2D Maxwell equations decouple into two polarization sets: the TM set, $E_x H_y E_z (D_x D_z)$, and the TE set $H_x E_y H_z (D_y)$. Each field set can be modeled independently of the other. For the 2D TM case, Eq. (2) can be rewritten using Eqs. (1) and (4) as follows:

$$\vec{D}(t) = \varepsilon_0 \vec{E}(t) - \varepsilon_0 \frac{\omega_p^2}{\Gamma}\left[\int_0^t \frac{1}{i\omega}\vec{E}(t')dt' - \int_0^t e^{-(t-t')\Gamma}\vec{E}(t')dt\right]. \quad (5)$$

Equation (5) is substituted into Eq. (1) with a tightly focused ultrashort pulsed Gaussian beam following the Eq. of

$$I_S(x,z,t) = \tau_d \times e^{-\left[\frac{(t-t_0)^2}{\tau_w^2}\right]} e^{i\omega m\Delta t} \times e^{-\left[\frac{x-\Delta u\times(D/2)}{w_0}\right]^2} \times e^{ik\sqrt{f_z^2+(x-D/2)^2}-f_z}$$

$$\tau_d = \frac{1}{2}\times\left[1+erf\left\{\frac{(m-20)}{5\sqrt{2}}\right\}\right] \quad (6)$$

where, the where t_0 is the pulse duration, τ_w is the pulse width, f is the focal length, D_x is the aperture diameter of the objective lens, w_0 is the full width half maximum (FWHM) value of the incident Gaussian beam, k (=2π/λ) is the wave number, m is the iteration number, and *erf* is the error function [30].

For absorbing boundary conditions (ABCs) in order to truncate the FDTD computational domain on dispersive media we employed Berenger's highly effective ABC, the perfectly matched layer (PML), which gives zero reflection at the absorbing boundary for all frequencies and all angles of incidence [31]. For the TM case, if H_y is known, then E_x and E_z can be calculated at the cross-sectional plane of the FDTD grid. Using plane wave propagation techniques, all the field components can be determined at a plane of interest well past the FDTD computational grid. To analyze the frequency response of the FDTD simulation results we can simply take the far-field Fourier transform of the E-field for all the time-domain data at every point of interest. This can be done by the equation

$$E(f_m) = \int_0^{t_T} E(t)\cdot e^{-j2\pi f_m t}dt\,, \quad (7)$$

where f_m is the frequency of interest and t_T is the final time step number of the FDTD iteration. This Eq. (6) can be divided into its real and imaginary parts. From these results we can determine the amplitude and phase information at the frequency f_m.

The Poynting vector $\vec{S}$ is given by $\vec{S} = S_x\hat{x} + S_z\hat{z} = \left(\vec{E}\times\vec{H}^*\right)/2$. In our TM case for SPR excitation $S_x = -\left(E_z H_y^*\right)/2$ and $S_z = \left(E_x H_y^*\right)/2$. Also, using the Maxwell's equations, electromagnetic quantities such as the electric and magnetic energy within the FDTD computational grid may be calculated. The Poynting (electromagnetic energy) flow describes power [W/m^2]. To obtain the total energy flow inside a region of interest we integrated all the directions of the Poynting flow and the given excited pulsed time periods including the focalized region.

$$W = \iiint \vec{S}\cdot\vec{n}da = -\int\int_{\substack{volume\\time}}\left(\vec{E}\cdot\vec{J} + \vec{H}\cdot\frac{\partial\vec{B}}{\partial t}\right)dtdv \quad (8)$$

As the energy density of the external field $\vec{S}_0 = \omega\varepsilon_2 E_0^2/2k$ was integrated during the excited Gaussian bema pulse duration, the total-field scattered-field and absorption cross section are given by $Q_{sca} = W/\vec{S}_0 = k^4|\alpha|^2/6\pi$, $Q_{abs} = k\,\mathrm{Im}(\alpha)$, respectively. The polarizability α can be obtained by the relation of the dipole moment $\wp$ and the complex dielectric constant of the surrounding medium ε_2, $\alpha = \wp/(\varepsilon_2 E_0)$ using the well-known Mie theory. In our case of the frequency-dependent FDTD, the absorption quantity Q_{abs} is defined by the integrated energy including the metal NPs divided by their volume or area fraction.

3. SIMULATION RESULTS

Figure 2(a) shows the z-directional Poynting energy was propagated tightly focused Gaussian pulsed beam with the excitation wavelength of 780nm and high numerical aperture objective lens of 1.4 (oil) inside a polymer matrix. Figure 2(b)-2(d) shows the refractive index distributions of our simulated Au metal only and hetero-structured Au-dielectric-Au/hollow inside a polymer matrix. .

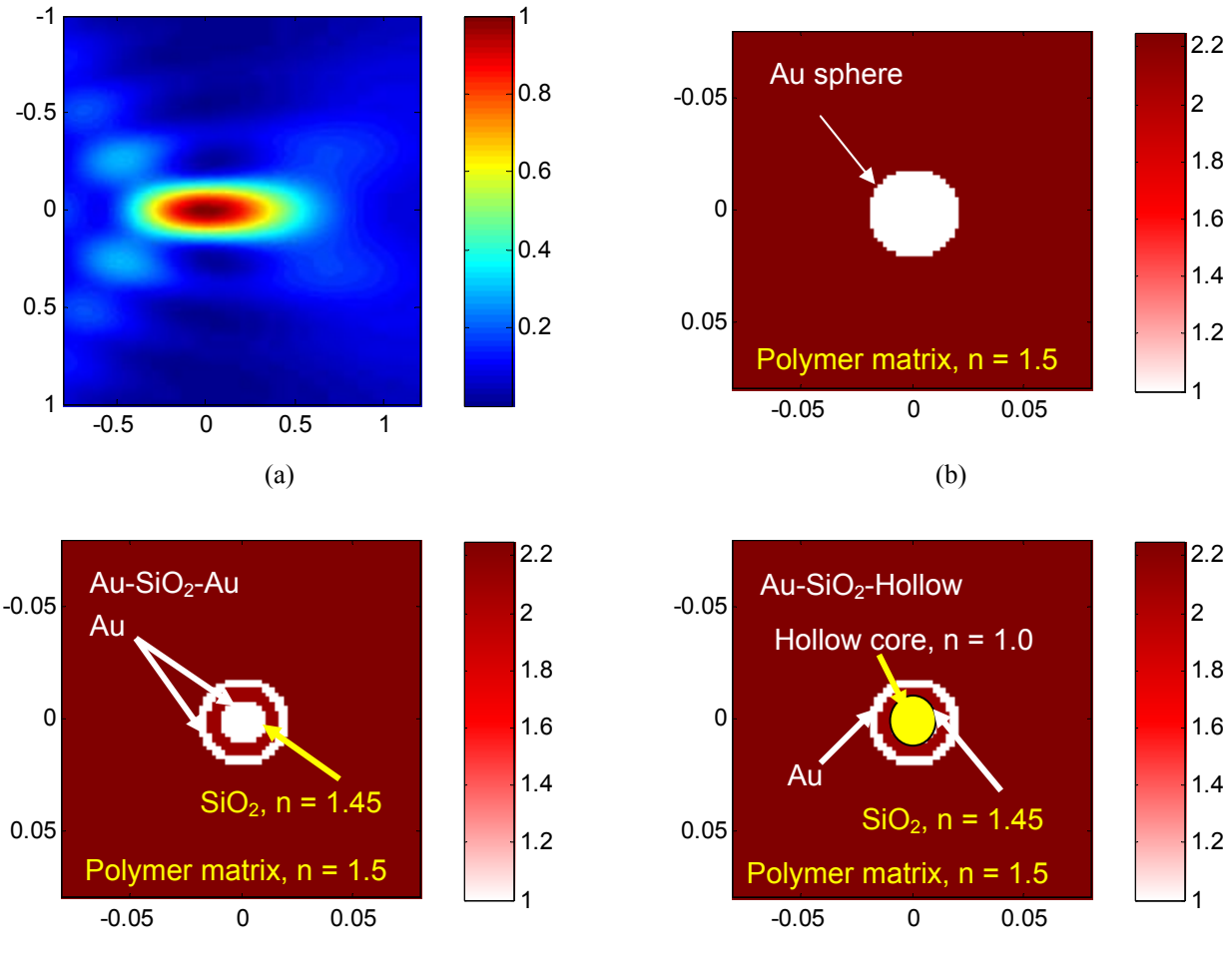

Figure 2. (a) z-directional Poynting energy of the tightly focused Gaussian pulsed beam with the excitation wavelength of 780nm and high NA objective lens of 1.4 inside a polymer matrix. Refractive index distributions of the simulated structures of (b) Au metal sphere with the diameter of 40 nm, (b) Au-SiO_2-Au heterostructure with the radius of 10 nm, 16 nm, and 20 nm, respectively, and (c) Au-SiO_2-Hollow core structure inside a polymer matrix.

For accurate comparison of each metal NP structures we used the same maximum diameter of 40 nm. The hetero structures are composed of the Au or hollow core of diameter 20 nm, SiO_2 inner shell with the thickness of 12 nm, and the Au outer shell with the thickness of 8 nm, respectively. To obtain the absorbance and enhanced near-field strength, we calculated the different shaped single NP structures with respect to different wavelength ranges covering from 400 nm to near infra-red wavelength of ~ 900 nm with wavelength steps of 5 nm. Figure 3 shows the obtained absorbance and maximum enhanced near-field SPR extinction efficiency of a single nano-sphere and hetero structures results from our frequency-dependent FDTD calculation and Poynting energy theorem under a Gaussian pulsed plane wave excitation condition. The near-field SPR enhancement factor $Q_{nf,max}$ was defined by the ratio of the maximum SPR

energy value divided by the maximum energy value of the incident Gaussian pulsed beam we could easily obtain the absorbed energy ratio of the random distributed NPs.

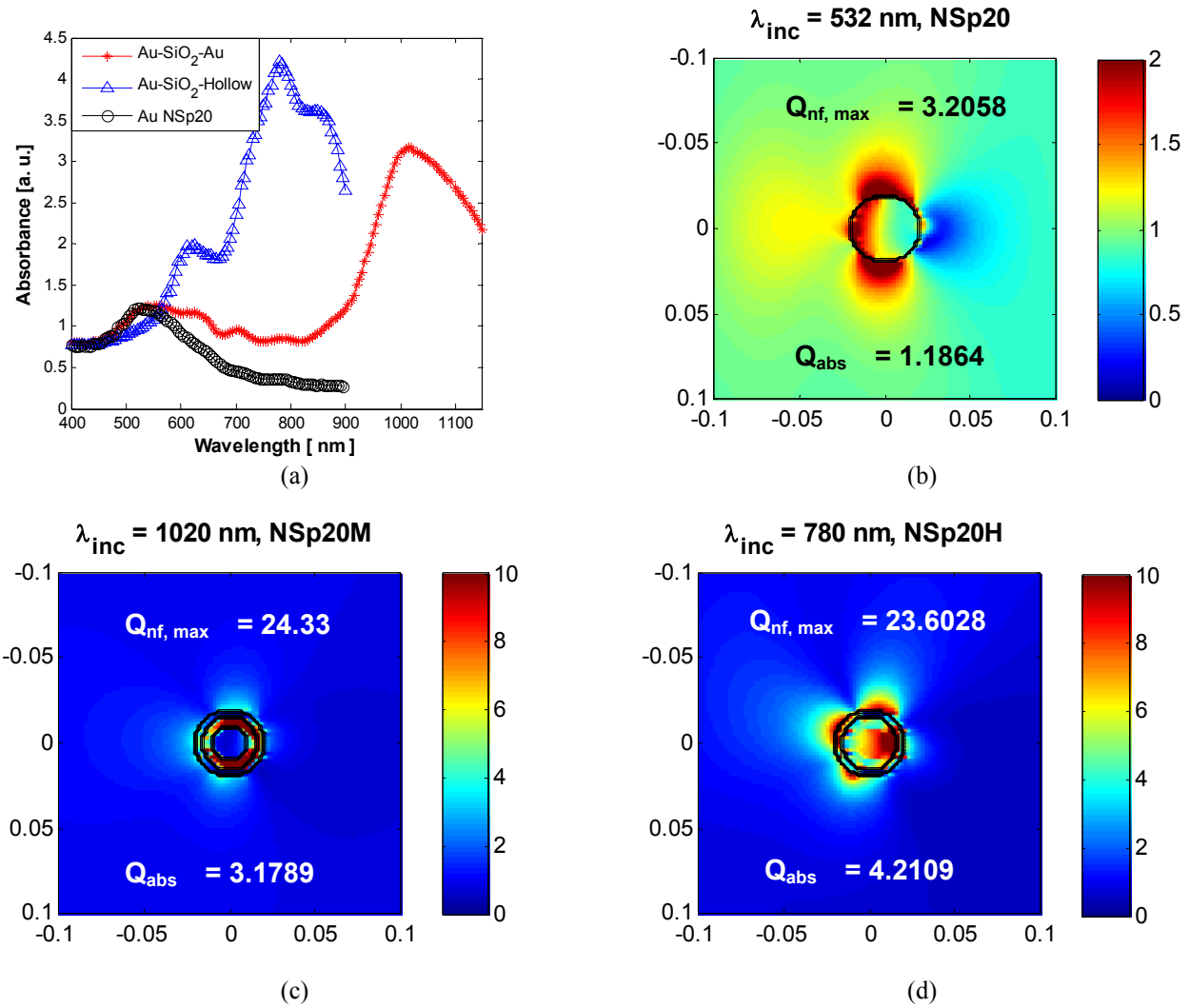

Figure 3. The calculated absorbance (a) and near-field SPR enhanced extinctions of (b) a single nano-sphere with the diameter of 40 nm, (c) Au-SiO_2-Au heterostructure with the radius of 10 nm, 16 nm, and 20 nm, respectively, and (d) Au-SiO_2-Hollow core structure from our frequency-dependent FDTD calculation under a Gaussian pulsed plane wave excitation condition.

As can be seen in the Fig. 3(a) the SPR-band matched absorption peak was found at 520 nm in case of the single Au nanosphere with the diameter of 20 nm. This result was well matched with Mie calculation and experimentally obtained absorbance data as well. The hetero-structured Au-SiO_2-Hollow core and Au-SiO_2-Au show the SPR peaks at the 780 nm and 1020 nm, respectively. In SPR absorption and excitation band engineering point of view, the SPR peak is very important for excitation source selection and conversion efficiency decision for spontaneous near-field enhancement energy and photo-thermal effect of the metallic NP doped system.

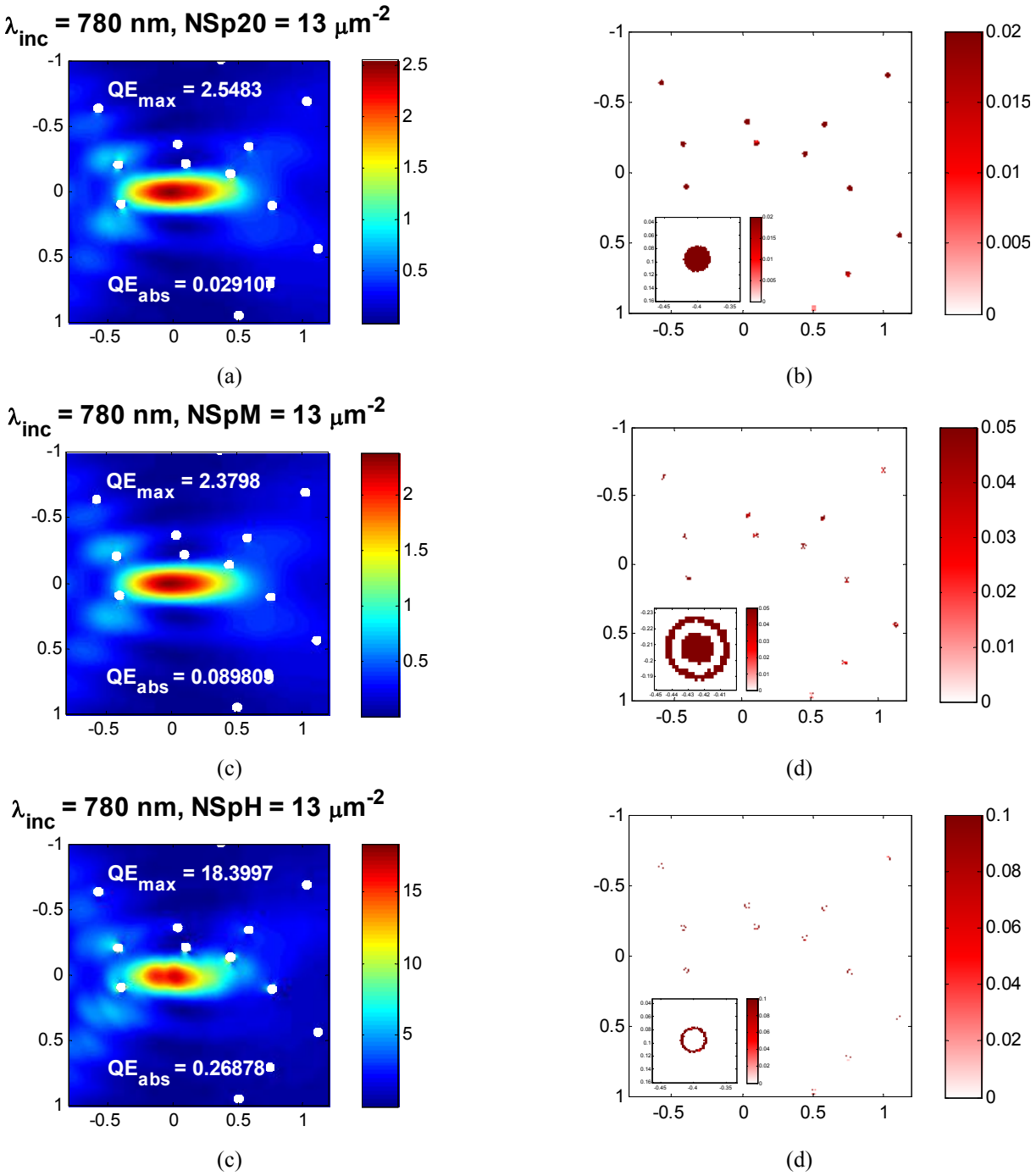

Figure 4. The calculated absorbance (a) and near-field SPR enhanced extinctions of a single nanosphere with the diameter of 40 nm (b), Au-SiO_2-Au heterostructure with the radius of 10 nm, 16 nm, and 20 nm, respectively (c), and Au-SiO_2-Hollow core structure (d) from our FDTD calculation results under a plane Gaussian pulsed wave excitation condition.

To model and apply a practical experimental condition, we assumed that the tightly focused (NA1.4, oil immersion) ultrashort pulsed laser irradiation condition with the wavelength of 780 nm and same positioned 1 or 2 particles concentration inside the focal volume were assigned in our frequency-dependent FDTD simulation. Figure 4 shows the

frequency-dependent FDTD simulation results under the tightly focused ultrashort pulse laser excitation and their extracted heat source distribution resulted from the absorbed energy of the random distributed metal NPs inside a polymer matrix. From the FDTD simulation result, we could notice and extract the enhanced localized near-field SPR maximum factor exactly. Because we assumed the maximum energy of the tightly focused Gaussian beam one, we could get the total-sum absorbed energy ratio of 0.02910:0.08980:0.02688=1:3.0859:9.2371=Au:Au-SiO_2-Au:Au-SiO_2-Hollow. From the SPR absorption band matched Au-SiO_2-Hollow structure, we could get the enhanced absorbance of at least 9-folds than the Au nanosphere only case. Such enhancement in heterostructures are thought to be due to the metal shell-metal core resonant plasmon coupling [7].

Since the field enhancement shown in Fig. 3 and 4 are highly localised within the nanoparticle structures, it is possible to induce localised surface ablation and deformation of nanoparticle shape even below the melting temperature of Au. Previously, Plech et. al. [32] have observed the surface ablation of nanospheres even at moderate pump pulse energies. Such ablation is supposed to be an extremely fast process (~ ps regime), which occurs before the thermalization of energy to the lattice of gold. The applications that could benefit from such highly localised fields are photodynamic cancer therapy and micro-void explosions in polymer. In photodynamic therapy, the surface ablation could be used to produce shock wave which could destroy the cells near-by. In void generations, again surface ablation could drive the micro-explosions. Both processes could benefit from low threshold power, due to highly localised SPR induced near-field enhancement. Further experimental studies are under way to test the feasibility of such applications.

5. CONCLUSION

We have simulated the SPR induced enhanced near-field strengths at various nanoparticle structures - metal nanosphere and heterogeneous morphologies (such as metal - dielectric - metal core-shell structures), and compared their efficiencies to determine suitable shape factors required for near-field enhanced surface ablation applications. Unlike the previous approximate analytical models, the SPR excitation and consequently near-field enhancement efficiencies are numerically simulated, using the frequency-dependent FDTD method under tightly focused ultrashort pulse laser irradiation to accurately emulate the experimental conditions. The calculated SPR absorbance results from our frequency-depended FDTD and Poynting energy theorem is well matched with the experimentally obtained data. The Au-SiO2-Au hetero-structure is found to be most efficient in near-field enhancement. Such enhancement could be due to the metal shell-core plasmon coupling. Further optimization of such structures is needed for future application. The near-field enhancement could be applied in photodynamic therapy and micro-explosions, where low threshold ablations are needed.

ACKNOWLEDGMENT

We are grateful thanks to the Centre for Astrophysics and Supercomputing (CAS) at Swinburne University of Technology for supporting the computing resources. The authors acknowledge the support for the Australian Research Council.

REFERENCES

1. H. Raether, Surface Plasmons on Smooth and Rough Surfaces and on Gratings, (Springer-Verlag, Berlin, 1988).
2. A. V. Zayats, I. I. Smolyaninov, and A. A. Maradudin, "Nano-optics of surface plasmon polaritons," Phys. Reports 408, 131-314 (2005).
3. J. Homola, S. Yee, and G. Gauglitz, "Surface plasmon resonance sensors: review," Sens. Actuators B 54, 3-15 (1999).
4. B. Rothenhausler and W. Knoll, "Surface plasmon microscopy," Nature 332, 615-617 (1988).
5. W. L. Barnes, A. Dereux, and T. W. Ebbesen, "Surface plasmon subwavelength optics," Nature 424, 824-830 (2003).
6. P. Andrew and W. L. Barnes, "Energy transfer across a metal film mediated by surface plasmon polaritons," Science 306, 1002-1005 (2004).

7. S. Lal, S. Link, and N. J. Halas, "Nano-optics from sensing to waveguiding," Nature photonics 1, 641-648 (2007).
8. S. A. Kalele, N. R. Tiwari, S. W. Gosavi, and S. K. Kulkarni, "Plasmon-assisted photonics at the nanoscale," J. Nanophotonics 1, 1-19 (2007).
9. O. J. F. Martin, C. Girard, and A. Dereux, "Generalized field propagator for electromagnetic scattering and light confinement," Phys. Rev. Lett. 74, 526-529 (1995).
10. C. Hafner, The Generalized Multiple Multipole Technique for Computational Electromagnetics, (Artech House, Boston, 1990).
11. A. Taflove and S. C. Hagness, Computational Electrodynamics: The Finite-Difference Time-Domain Method, 2nd ed., (Artech House, Boston, 2000).
12. R. X. Bian, R. C. Dunn, and X. S. Xie, "Single molecule emission characteristics in near-field microscopy," Phys. Rev. Lett. 75, 4772-4775 (1995).
13. Y. Xie, A. R. Zakharian, J. V. Moloney, and M. Mansuripur, "Transmission of light through a periodic array of slits in a thick metallic film," Opt. Express 13, 4485-4491 (2005).
14. J. M. López-Alonso, J. M. Rico-García, and J. Alda, "Photonic crystal characterization by FDTD and principal component analysis," Opt. Express 12, 2176-2186 (2004).
15. S. Chang and A. Taflove, "Finite-difference time-domain model of lasing action in a four-level two-electron atomic system," Opt. Express 12, 3827-3833 (2004).
16. R. C. Gauthier, "Computation of the optical trapping force using an FDTD based technique," Opt. Express 13, 3707-3718 (2005).
17. R. Drezek, A. Dunn, and R. Richards-Kortum, "Light scattering from cells: finite-difference time-domain simulations and goniometric measurements," Appl. Opt. 38, 3651-3661 (1999).
18. J. B. Judkins, R. W. Ziolkowski, and C. W. Haggans, "Two-dimensional finite-difference time-domain simulation for rewritable optical disk surface structure design," Appl. Opt. 35, 2477-2487 (1996).
19. D. W. Prather and S. Shi, "Formulation and application of the finite-difference time-domain method for the analysis of axially symmetric diffractive optical elements," J. Opt. Soc. Am. A 16, 1131-1142 (1999).
20. K. S. Yee, "Numerical solution of initial boundary value problems involving Maxwell's equations," IEEE Trans. Antennas Propag. 14, 302-307 (1966).
21. E. D. Palik, Handbook of Optical Constants of Solids, (Academic, New York, 1985).
22. M. Fox, Optical Properties of Solids, (Oxford University Press, New York, 2001).
23. R. J. Luebbers, F. P. Hunsberger, K. Kunz, R. Standler, and M. Schneider, "A frequency-dependent finite difference time domain formulation for dispersive materials, " IEEE Trans. Electromagn. Compat. 32, 222-227 (1990).
24. D. F. Kelley and R. J. Luebbers, "Piecewise linear recursive convolution for dispersive media using FDTD," IEEE Trans. Antennas Propagat. 44, 792-797 (1996).
25. T. Kashiwa and I. Fukai, "A treatment by FDTD method of dispersive characteristics associated with electronic polarization," Microwave Opt. Tech. Lett. 3, 203-205 (1990).
26. D. M. Sullivan, "Frequency-dependent FDTD methods using Z transforms," IEEE Trans. Antennas Propagat. 40, 1223-1230 (1992).
27. M. Born and E. Wolf, Principles of Optics, 7th ed., (Cambridge University Press, Cambridge, 1999).
28. P. Drude, " Zur Elektronentheorie der Metalle,"Ann. Phys. 1, 566-613 (1900).
29. M. I. Markovic and A. D. Rakic, "Determination of the reflection coefficients of laser light of wavelengths λ_e (0.22 μm, 200 μm) from the surface of aluminum using the Lorenz-Drude model," Appl. Opt. 29, 3479-3483 (1990).
30. K. Choi, J. W. Chon, M. Gu, and B. Lee, "Characterization of a subwavelength-scale 3D void structure using the FDTD-based confocal laser scanning microscopic image mapping technique," Opt. Express 15, 10767-10781 (2007).
31. J. P. Berenger, "A perfectly matched layer for the absorption of electromagnetic waves," J. Comput. Phys. 114, 185-200 (1994).
32. A. Plech, V. Kotaidis, M. Lorenc, J. Boneberg, "Femtosecond laser near-field ablation from gold nanoparticles," Nature Physics 2, 44-47 (2006).